

FLOW AND HEAT TRANSFER FOR JET IMPINGEMENT ARRAYS WITH LOCAL EXTRACTION

Andrew J. Onstad, Terri B. Hoberg, Christopher J. Elkins, and John K. Eaton

Department of Mechanical Engineering,
488 Escondido Mall, Building 500
Stanford University, Stanford, California, 94305, USA
aonstad@stanford.edu, eatonj@stanford.edu

ABSTRACT

Multiple jet impingement cooling systems are preferred over single jets because they offer higher and more uniform mean heat transfer. Unfortunately, multiple jet systems can suffer from crossflow which is the interaction of the spent fluid with downstream jets. The present work examined impingement arrays in which the spent fluid was removed through local extraction holes. Three different impingement arrays were studied all of which had jet-to-jet spacing of $Z_n/D = 2.34$, jet-to-target spacing of $H/D = 1.18$, and extraction holes in the jet plane. Magnetic Resonance Velocimetry, MRV, is used to measure the mean velocity field in the largest array. Mean heat transfer measurements were carried out as a function of the jet Reynolds number, Re_D , on the first array as well as two additional arrays to examine the effect of the extraction area ratio and the geometric scaling. The Nusselt number, Nu_D , was shown to have the same functional relationship with the Reynolds number for all three arrays. Also, Nusselt number scaling indicates that very large heat transfer coefficients could be obtained with arrays of small jets.

INTRODUCTION

Jet impingement cooling is a broadly accepted method of heat transfer because of the very high local heat transfer coefficients that are possible. Both single and multiple jet systems are used however, multiple jet systems are gaining more popularity in application because they provide higher and more uniform mean heat transfer. Unfortunately, the heat transfer coefficient in these multiple jet arrays is adversely affected by the fluid which has already impacted the target surface, or the spent fluid. The central jets impact the target surface and their fluid then interacts with the surrounding jets producing a situation commonly referred to as crossflow. The effect of crossflow in reducing the heat transfer coefficient has been examined by Kercher and Tabakoff (1970) and Florschuetz (1981) among others. Kercher and Tabakoff (1980) proposed a mean Nusselt number correlation for arrays of jets as a function of the Reynolds number, hole geometry, and the effect of spent

fluid. Florschuetz (1981) proposed a correlation of a similar form however, a coefficient was included to account for the effect of the crossflow.

The effect of crossflow can be minimized by extracting the spent fluid before it is allowed to degrade the heat transfer of the entire array. Gas turbine blade geometries allow for local extraction through film cooling holes located on the cooled target surface, Figure 1.

In this paper, an alternative approach is examined where the spent fluid is removed locally to a plenum through extraction holes placed on the same surface as the exit of the impingement jets as shown in Figure 2. This geometry is more feasible for electronics cooling applications.

There have been several previous reviews examining both single and multiple jet impingement; most notably Martin (1977), Downs and James (1987), Jambunathan et al. (1992), Viskanta (1993), and Han and Goldstein (2001). Relatively little published research has been done regarding multiple jet impingement with local extraction of the spent fluid to a plenum. Rhee et al. (2003b) examined the effect of the exhaust hole pattern on the geometry described in Figure 1. They showed the configuration with the largest extraction area to jet area (A_e/A_{jet}) consistently achieved higher heat transfer coefficients at every separation distance (H/D) tested.

Huber and Viskanta (1994a) examined the effect of the ratio of jet height to jet diameter, H/D , on the geometry pictured in Figure 2. The average heat transfer rate was found to increase 10% when using local extraction as compared to no extraction for small separation distances, $0.25 \leq H/D \leq 1$. Although the heat transfer rates for extracted and non-extracted arrays were found to be similar for $H/D = 1$, Huber and Viskanta (1994a) concluded that at separation distances less than 2, increased heat transfer rates would be expected. Rhee et al. (2003a) studied a staggered geometry by a naphthalene sublimation method. They showed that the average heat transfer coefficient increased for separation distances less than 2. Further, they reported increases of 20% and nearly 60% for $H/D = 1$ and $H/D = 0.5$, respectively. In another study by Huber and Viskanta (1994b), the effect of jet-to-jet spacing, Z_n ,

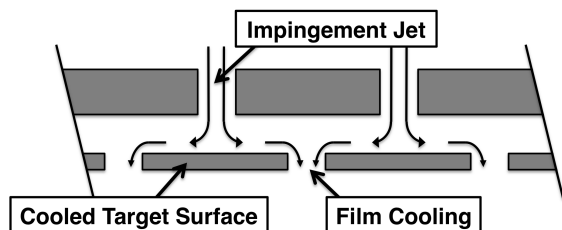


Figure 1: Local extraction from the target surface.

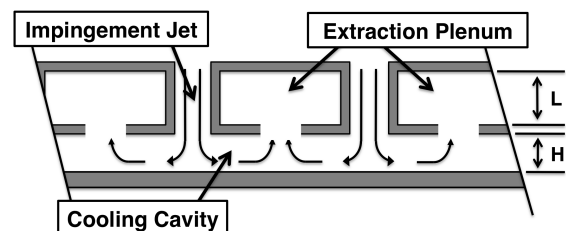


Figure 2: Local extraction from the impingement plane.

was examined. The mean heat transfer coefficient increased with decreasing jet-to-jet spacing for all three configurations tested, $Z_n/D = \{4, 6, 8\}$. Although the smallest array had the highest heat transfer coefficient, it also required the highest mass flow rate.

Very high heat flux electronics cooling applications could utilize impingement geometries with small jet-to-jet spacings. Reducing the inter-jet spacing, Z_n/D , will maximize the number of jets impacting the target surface increasing the array's ability to remove heat. Both Huber and Viskanta (1994a,1994b) and Rhee et al. (2003a) showed increased heat transfer with decreasing jet-to-jet spacing however, their studies were not compact enough with $Z_n/D = 4$ and $Z_n/D = 6$ respectively. In addition, decreasing the jet-to-jet spacing will increase the array's susceptibility to crossflow. Thus, a geometry which incorporates local extraction with a large exhaust area ratio, A_e/A_{jet} , is preferred to maintain a high average transport coefficient. With this in mind, the purpose of this research was two-fold: (1) to experimentally measure the mean flow field of a compact impingement geometry ($X_n/D_{jet} = 2.34$) with local extraction of spent fluid ($A_{spent}/A_{jet} = 2.23$) by way of Magnetic Resonance Velocimetry (MRV), and (2) to measure the mean heat transfer coefficient as a function of jet Reynolds number, Re_D , for a series of impingement arrays which have been geometrically scaled by a factor of 3 to determine if these types of arrays will follow a simple Reynolds number, Re_D , type scaling. Understanding the scaling behavior will allow the design of optimal impinging jet systems. This work is an extension to that of Onstad et al. (2009). Flow field measurements shown here are used to explain the heat transfer behaviors. For a more detailed description of the spatially resolved, three-component flow field see Onstad et al. (2009).

EXPERIMENTAL APPARATUS & TECHNIQUES

Description of Geometry

Three different impingement geometries were used. One was imaged by MRV to measure the spatially resolved, 3D mean flow field, and two more were used to examine the scaling relationship between the Nusselt and Reynolds numbers. The impingement geometry, shown qualitatively in Figure 3, consists of a staggered array of injection holes with a jet-to-jet spacing, Z_n/D , of 2.34 jet diameters. Each interior injection hole is surrounded by 6 regularly spaced local extraction holes. This hole placement allows for an extraction hole located in the geometric center of any two injection holes. The jet-to-target distance, H/D , was maintained at 1.18 diameters for each array tested. Table 1 lists the specifications of the three arrays.

Array	D [mm]	d [mm]	A_e/A_{jet}	Z_n/D	H/D	L/D	Re_D
(1)	8.46	7.29	2.23	2.34	1.18	2.25	2000 - 10,000
(2)	8.46	5.08	1.08	2.34	1.18	2.25	2000 - 10,000
(3)	2.82	1.69	1.08	2.34	1.18	6.76	500 - 4000

Table 1: Impingement geometric specifications used in this study.

Figure 4 illustrates the impingement apparatus used in these experiments. The flow enters the inlet manifold from an approximately 0.5m long, 51 mm diameter development pipe. The flow turns 90° in the inlet manifold and is distributed across the the impingement array. The inlet manifold is tapered in order to make the jet mass flow rates even

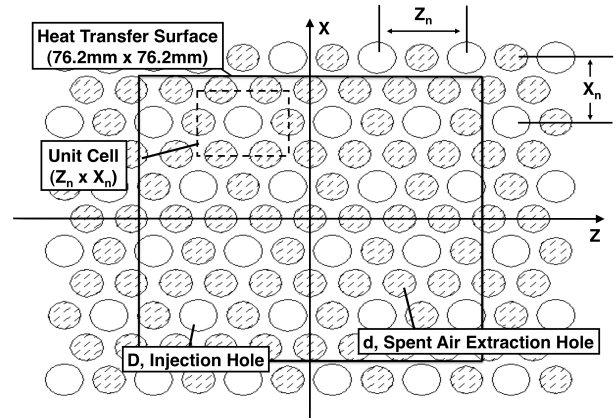


Figure 3: View of the jet impingement geometry from the jet impingement exit plane. The geometry is a staggered array of 36, injection holes of diameter D , each are surrounded by 6, extraction holes of diameter d .

by establishing a uniform pressure distribution on the tapered manifold wall. The flow travels 29 mm through the extraction manifold in individual tubes exiting in the cooling cavity as an array of jets. The jets impact the target surface at $y = 0$. Upon striking the target surface an array of radial wall jets are formed and the interaction of the wall jets forces the fluid away from the target surface and into the extraction plenum. The fluid flows around the injection tubes and out of one of four 25 mm tubes located in the corners of the plenum. These four extraction tubes combine and the flow exits through a 31.8 mm pipe. The entire apparatus is manufactured by stereolithography in plastic for compatibility with the MRV system and to minimize conduction heat transfer.

Magnetic Resonance Velocimetry

Magnetic Resonance Velocimetry (MRV) was used to measure the spatially resolved, three-component mean velocity field within array (1). MRV is a non-invasive experimental technique which utilizes the nuclear magnetic resonance (NMR) properties of Hydrogen atoms bound in water. The technique is capable of measuring the spatially-resolved, three-component mean velocity field inside of complex geometries without the use of flow tracers or requiring optical access (Elkins and Alley, 2007). The measurements were carried out in a 1.5T General Electric Signa CV/i magnetic

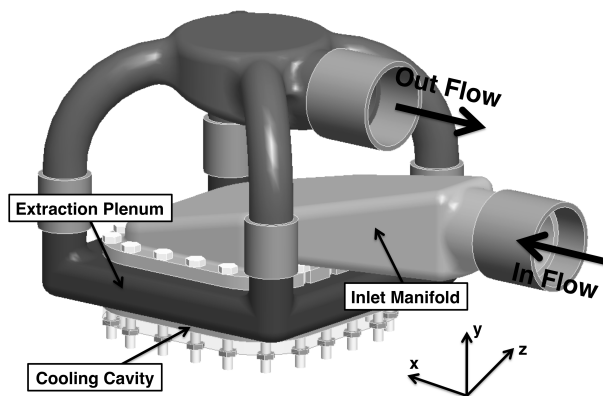


Figure 4: Isometric view of impingement apparatus showing the major components as well as the in and out flow directions.

resonance imaging system. The working fluid is contrast-enhanced water which is pumped from a holding reservoir by a centrifugal pump (Little Giant, TE-6MD-HC) through the impingement apparatus, located in the magnet bore, and back to the holding reservoir. The volume flow rate of water is measured during the experiment by a paddle-wheel flow meter where the estimated uncertainty is 4%. The MR images were found to have negligible interference from the pump and flowmeter.

Mean velocity measurements were averaged from 16 experiments at $Re_D = 5300$, (76 +/-3L/min). The total imaging volume of 240 mm x 64 mm x 240 mm (x, y, z) included the entire cooling cavity, impingement array, and a portion of the inlet manifold. The MRV measurements were performed with an isotropic spatial resolution of approximately 1 mm. The maximum uncertainty in individual mean velocity vectors from this technique was determined to be less than 10% by Elkins et al. (2004).

Heat Transfer

Average heat transfer measurements were carried out on all three impingement geometries. A 76.2mm square heat transfer surface was added to supply a constant wall temperature at the target surface plane ($y = 0$). The heat transfer surface was constructed of two oxygen-free, high thermal conductivity copper plates. One plate was flush mounted in an acrylic frame sealing the cooling cavity at $y = 0$. Five k-type thermocouples were mounted in holes drilled half way through the plate from the reverse side. A second OFHC plate was epoxied to the first OFHC plate sandwiching the thermocouples in between. Grooves cut in the first plate, allowed the thermocouples wires to escape. The thermocouples are located with one at the origin, $(x, z) = (0, 0)$ in Figure 3, and one in each of the four quadrants surrounding the origin, specifically $x = +/- 25.7$ mm, $z = +/- 24.8$ mm. The mean wall temperature, T_{wall} , was determined by averaging the five individual thermocouples. The readings from the five individual thermocouples were found to deviate less than 0.5 °C, thus, the average was believed to be a good representation of the mean wall temperature. A kapton heater (Omega, KH-303/10) was fixed to the back of the second OFHC copper plate in order to supply the necessary heat flux to the system. Power was supplied to the heater by a 110V variable AC transformer. Heater voltage drop was measured by a digital multimeter (Fluke, 8842A) and the current was measured using a wattmeter (Valhalla, 2101) wired in series with the load.

Compressed air from a filtered, dried, and temperature controlled source is used for the heat transfer experiments. The air passed through a 0.5 m long, 50.8 mm diameter development pipe and into the inlet manifold of the impingement apparatus. The air inlet temperature, T_{in} , was measured immediately upstream of the inlet manifold by a 1.57 mm diameter k-type thermocouple (Omega, KMQSS-062E-6) immersed parallel to the flow. A uniform inlet temperature is assumed because of several flow metering, control, and turning elements in addition to several meters of ambient temperature pipe upstream of the measurement. The air exit temperature, T_{exit} , is measured by another k-type thermocouple (Omega, KMQSS-062E-6) immersed in the flow downstream of the apparatus. Further downstream of the apparatus, the mass flow rate was measured by two identical 52.5 mm orifice plate meters positioned in parallel with each other. Three different square-edged orifice plates, $D_{bore} = 19.05$ mm, 25.40mm, 35.00mm, are used to obtain

a jet Reynolds number range of 2000 - 10,000 for arrays (1) and (2). A jet Reynolds number range of 500 - 4000 was achieved for array (3). Uncertainty in the mass flow rate and Reynolds number were both estimated to be less than 0.5% based on a 95% confidence interval using the method of Kline and McClintock (1953).

The mass flow rate was set to give the correct Reynolds number and the air inlet temperature was maintained at 23°C +/-0.1°C. Sufficient electrical power was supplied to the heat transfer surface to maintain a 30°C temperature differential between the wall and the inlet temperature. Once the temperature reading became steady, 50 voltage measurements were recorded from each thermocouple using an HP 3497A multiplexor and a Fluke 8842A digital multimeter both controlled via GPIB and referenced to an ice bath at 0.01 °C. Uncertainty in the temperature measurements was estimated at +/-0.2 °C based on a 95% confidence interval.

The jet Nusselt Number is defined as:

$$Nu_D = \frac{(\dot{q} - \dot{q}_{loss})D}{k_f A_{HT} (T_{wall} - T_{in})} \quad (1)$$

where \dot{q} is the input heating rate, k_f is the thermal conductivity of air, A_{HT} is the area of the heat transfer surface, and T_{wall} and T_{in} are the mean wall and air inlet temperatures respectively. Although the impingement apparatus is wrapped with 25.4 mm of thermal insulation to minimize heat losses, a heat loss term, \dot{q}_{loss} is also included in Eq. 1. In order to estimate this term, the experiment is stabilized at $Re_D = 10000$ with the heater power on. The air flow and the electrical power were turned off simultaneously, and the wall temperature decay was recorded. The heat losses were estimated by numerically differentiating the wall temperature decay. At $Re_D = 10000$, the losses are estimated at 2W. Because the wall temperature is the same at all flow rates, the loss estimation is assumed constant as well. The uncertainty in the loss estimate is conservatively set at +/-50% resulting in an uncertainty in the Nusselt number of +/-7% based on a 95% confidence interval.

RESULTS AND DISCUSSION

Magnetic Resonance Velocimetry

Fully 3-D, mean velocity measurements inside the cooling cavity were carried out at a Reynolds number of $Re_D = 5300$ based on the jet diameter. Figure 5 shows a close up view of contours of the mean velocity magnitude and in-plane, $z - y$, velocity vectors for a plane, $x = -25.4$ mm inside the cooling cavity. The figure shows a jet exiting the impingement array at approximately $y = 10$ mm with a velocity near 0.7 m/s. The jet spreads and slows before stagnating on the target surface at $y = 0$. The stagnation region immediately under the jet centerline is referred to as the primary stagnation region. The jet then turns radially outward accelerating along the target surface to a velocity near 0.3 m/s before it interacts with the radial wall jet from an adjacent impingement jet resulting in the secondary stagnation region. The locally high static pressure from the secondary stagnation pushes the fluid upward toward the local extraction hole at a velocity near 0.25 m/s. The fluid is then exhausted to the extraction plenum where the mean velocity magnitudes are low. The in-plane velocity vectors in Figure 5 show a smooth transition from the impingement jet to the radial wall jet and out of the cooling cavity without obvious vortical motion around the jet.

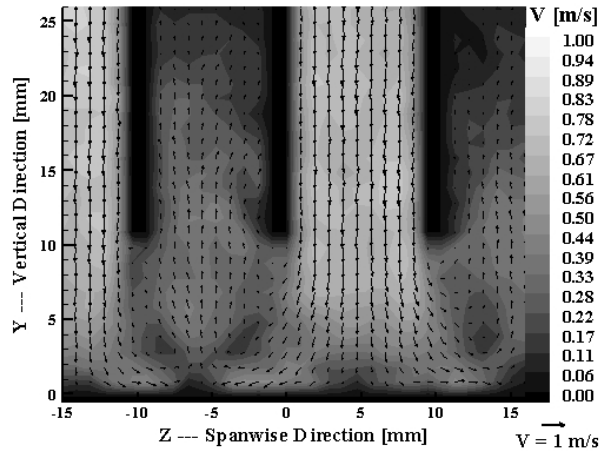


Figure 5: Velocity magnitude contours and in-plane, $(z - y)$, velocity vectors showing the flow field at $x = -25.4\text{mm}$.

Figures 6 and Figure 7 show contours of velocity magnitude and in-plane velocity vectors for $x - z$ planes inside the cooling cavity. For clarity in these two figures, the in-plane velocity vectors are shown at a spacing 2x the measurement resolution. Figure 6 shows a plane approximately 3 mm above the target surface, whereas Figure 7 is immediately above the target surface. These figures are distinctly different. Figure 6 shows a jet which entered the cooling cavity with a circular cross-section now having an elliptical cross-sectional shape. Around each jet, is a ring of little or no flow. Beyond the ring is a region of interconnected flow whose mean velocity is primarily opposite the jet with a magnitude near 0.25 m/s. This region is the upwelling of flow from the secondary stagnation moving toward the extraction holes. The in-plane velocity vectors in this upwelling show a slight mean velocity in the $-x$ direction. This mean velocity is a crossflow due to the shape of the tapered inlet manifold. The inlet manifold taper ends in a radius instead of reaching zero height. The result is that the stagnation pressure is not uniform in the manifold so there is slightly higher mass flow through the jets on the downstream side, $+x$, of the impingement array. This increased jet mass flow rate manifests itself as a crossflow inside the cooling cavity. Further examination quantified a jet mass flow rate variation of 15% in the x direction. In the cooling cavity, the mean jet velocity to crossflow velocity is 8%. The elliptical shape of the jets in Figure 6 is a result of this slight crossflow.

Figure 7 is measured immediately above the target surface and is markedly different that of Figure 6. Here, a primary stagnation region is visible on each jet centerline. An axisymmetric wall jet accelerates fluid away from the primary stagnation. A secondary stagnation formed from the interaction of adjacent wall jets results in a hexagon like region of no flow around each jet. This region corresponds very well to the upwelling of flow shown in Figure 6. These two regions have different effects on heat transfer, the primary stagnation region enables high heat transfer coefficients due to a very thin boundary layer. The secondary stagnation however, will degrade the local heat transfer coefficient by keeping warm fluid near the wall.

Heat Transfer

Average heat transfer measurements were carried out as function of the jet Reynolds number for all three arrays specified in Table 1. Figure 8 shows the average Nusselt number,

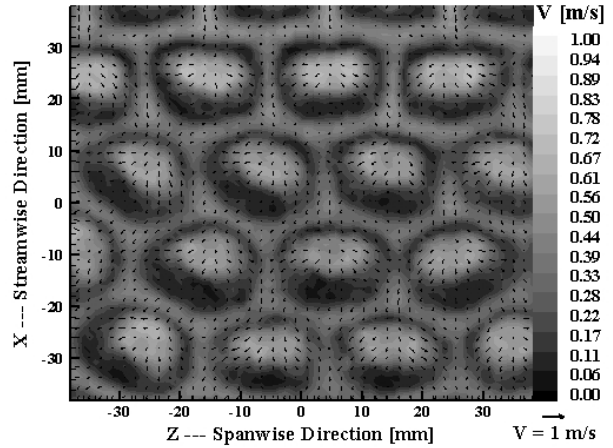


Figure 6: Velocity magnitude contours and in-plane, $(x - z)$, velocity vectors showing the flow field at $y = 3\text{mm}$.

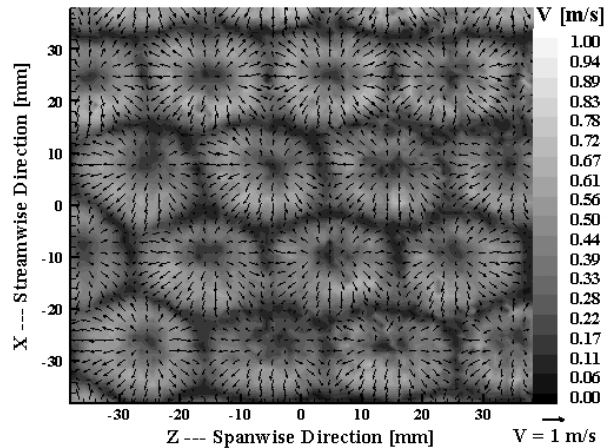


Figure 7: Velocity magnitude contours and in-plane, $(x - z)$, velocity vectors showing the flow field at $y = 0$.

Nu_D , as function of the jet Reynolds number for all three arrays. Array (1), in squares, and array (2), in triangles, have identical jet diameters with the same total number of jets. They only differ in the extraction area ratio, A_e/A_{Jet} , where array (1) has over a factor of 2 greater extraction area ratio. From Figure 8, arrays (1) and (2) appear to have nearly identical power law dependence of Nusselt number with Reynolds number, yet array (2) has a Nusselt number that is on average 9% higher than array (1) at every Reynolds number tested. We see that the extraction area ratio has a weak but consistent effect on the Nusselt number, yet it has little influence on its power law relationship with the jet Reynolds number. This result contradicts the findings of Rhee et al. (2003b) for a case where the extraction holes are located on the heat transfer surface as in Figure 1. They found an increase in Nu with increasing extraction area. However, they compared extraction area ratios of different array geometries, not of arrays of the same geometry. In the present case, a reduction in extraction area ratio will increase the extraction velocity of array (2) by a factor of 2 because the jet areas and thus flow rates are identical. The higher velocity results in increased pressure drop through the exhaust holes. This would tend to reduce the crossflow in the cooling cavity since the pressure drop in the uniformly distributed exhaust holes would play a bigger role in controlling the distribution of flow rates. Having smaller exhaust

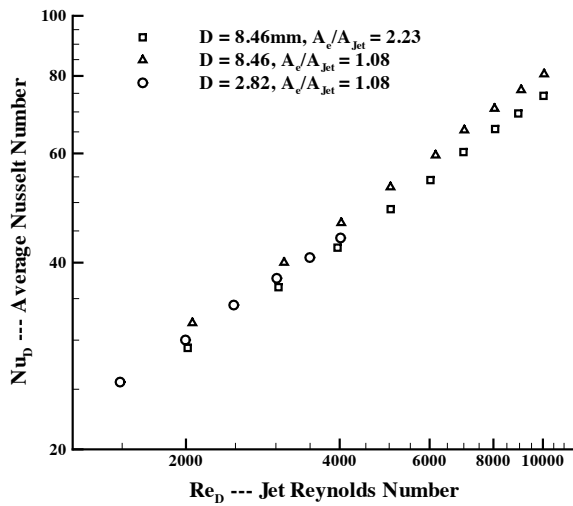


Figure 8: Mean Nusselt number, Nu_D , versus the jet Reynolds number, Re_D .

holes may also reduce the size of the secondary stagnation areas slightly.

Heat transfer results for array (3) are also shown in Figure 8 as circles. The Nusselt number curve is similar to arrays (1) and (2) however, the power law dependence on the Reynolds number is not as strong. It is important to note that array (3) is not a perfect geometric scaling of array (2). The height of the exhaust manifold (L in Figure 2) is identical for both arrays. In other words, it is not scaled to the hole diameter. Therefore, the results indicate that L/D has at most a small effect on the Nusselt number. Dimensionally, this means scaling the entire geometry by a factor of three does enable factor of three increase in the mean heat transfer coefficient. Unfortunately, the increase in the heat transfer coefficient requires a factor of three increase in mass flow rate at the same Reynolds number.

Coefficients for a power law fit, Eq. 2, to the Nusselt number data are shown in Table 2.

$$Nu_D = C_o Pr^{1/3} Re_D^b \quad (2)$$

Array	D [mm]	d [mm]	A_c/A_{jet}	C_o	b
(1)	8.46	7.29	2.23	0.376	0.586
(2)	8.46	5.08	1.08	0.436	0.579
(3)	2.82	1.69	1.08	0.602	0.531

Table 2: Empirical constants for a power law relationship of Nu_D versus Re_D .

The compact jet-to-jet spacing, $Z_n/D = 2.34$, of these arrays continued the trend documented by Huber and Viskanta (1994b) of increasing mean Nusselt number with decreasing jet-to-jet spacing. The performance of these arrays is an approximately 10% improvement over the most compact array tested by Huber and Viskanta (1994b) of $Z_n/D = 4$. Increasing the mean heat transfer by decreasing the jet-to-jet spacing however, comes at the expense of an increase in the mass flow rate per heat transfer area requirement.

A comparison of the results of this study with results from previous correlations from Martin (1977) and

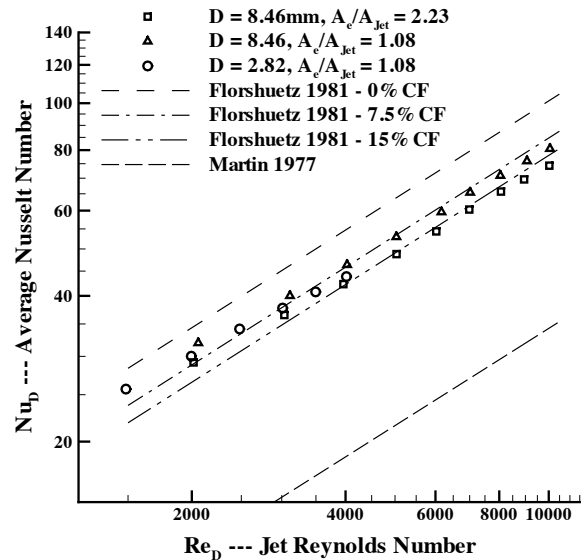


Figure 9: Mean Nusselt number, Nu_D , versus the jet Reynolds number, Re_D . Model curves plotted from Florschuetz et al. (1981) and Martin (1977).

Florschuetz et al. (1981) are shown in Figure 9. The correlation by Martin (1977) considers the geometry however, it does not account for any crossflow. Florschuetz et al. (1981) considers both the geometry and crossflow and is shown for three different crossflow-to-jet velocity ratios, 0%, 7.5%, and 15%. The correlation provided by Martin (1977) over predicts the strength of the relationship between the Nusselt number and the Reynolds number. In addition, the magnitude of the Nusselt number predicted by Martin (1977) is much too low at every Reynolds number tested. At Reynolds number less than about 5000, the model by Florschuetz et al. (1981) with a 7.5% crossflow-to-jet velocity ratio does a reasonable job at predicting the magnitude of the Nusselt number. The model however, over predicts the effect of the Reynolds number leading to an increasing error for increasing Reynolds numbers. The geometry tested does not fit within the range of geometric parameters provided by Martin (1977, $0.004 \leq A_{jet}/A_{HT,Unit} \leq 0.04$, and $2 \leq H/D \leq 12$, or in the jet spacing parameters provide by Florschuetz et al.(1981), $5 \leq Z_n/D \leq 10$, and $4 \leq X_n/D \leq 8$, thus it is expected that they may not capture the behavior of these more compact arrays.

CONCLUSION

Measurements of the fully 3-D, mean velocity field within a compact, jet impingement array with local extraction of the spent fluid are presented. These measurements show a smooth transition from the impingement jet to an axisymmetric radial wall jet whose interaction with adjacent wall jets forces the fluid out of the cooling cavity through appropriately placed local extraction holes. The secondary stagnation regions were shown to resemble a hexagonal shape around each jet due to the choice of a staggered array of jets. In the case of heat transfer, it is preferable to minimize heat transfer surface area covered by the secondary stagnation due to its adverse effects on the mean heat transfer coefficient. Further, an appreciable crossflow velocity in the cooling cavity was measured at 8% of the jet velocity. The jet mass flow rate variation was approximately 15%, thus it

is suspected the inclusion of local extraction in this geometry minimized the effect of the non-uniformity. Although not intended, this type of non-uniform inlet boundary condition may be likely in practice. Further, the inclusion of local extraction in the manufacture of jet impingement arrays may help in minimizing the adverse effects of crossflow.

The mean Nusselt number was obtained as a function of the jet Reynolds number for three different arrays. The first and second arrays differed in the extraction area ratio, whereas the second and third were geometrically scaled by a factor of 3. The decrease in the extraction area ratio increased the mean Nusselt number magnitude by about 9% but had little effect on its power law dependence on Reynolds number. As long as the pressure drop required to push the fluid into the extraction plenum is much smaller than the pressure drop necessary to push the fluid around the jets in the cooling cavity, the overall effect of changing the extraction area ratio on the thermal performance of the array will be small. In addition, measurements of the mean Nusselt number as a function of the jet Reynolds number for geometrically scaled arrays were shown to have very similar behavior. We have shown that decreasing the scale of the impingement array geometrically by a scale factor does increase the heat transfer coefficient based on the jet diameter by the same geometric factor, in the case of this study a factor of three. The cost of the increased performance comes in the form of an equal increase in the mass flow rate requirement at a specified Reynolds number. This scaling relationship will be helpful in deciding how to relate experiments of mean heat transfer performance of large arrays to the much smaller ones likely to be used in electronics cooling applications.

REFERENCES

- Downs, S. J., and E. H. James, 1987. "Jet Impingement Heat Transfer - A Literature Survey," *American Society of Mechanical Engineers*, 87-HT-35.
- Elkins, C. J., and M. T. Alley, 2007, "Magnetic Resonance Velocimetry: Applications of Magnetic Resonance Imaging in the Measurement of Fluid Motion," *Experiments in Fluids*, **43**(6) pp. 823-858.
- Elkins, C. J., M. Markl, A. Iyengar, R. Wicker, and J. K. Eaton, 2004, "Full-Field Velocity and Temperature Measurements Using Magnetic Resonance Imaging in Turbulent Complex Internal Flows," *International Journal of Heat and Fluid Flow*, **25**(5) pp. 702-710.
- Florschuetz, L. W., C. R. Truman, and D. E. Metzger, 1981, "Streamwise Flow and Heat Transfer Distributions for Jet Array Impingement with Crossflow," *Journal of Heat Transfer*, **103** pp. 337-342.
- Han, B., and R. J. Goldstein, 2001, "Jet-Impingement Heat Transfer in Gas Turbine Systems," *Annals of the New York Academy of Sciences*, **934** pp. 147-161.
- Huber, A. M., and R. Viskanta, 1994a, "Convective Heat Transfer to a Confined Impinging Array of Air Jets with Spent Air Exits," *Journal of Heat Transfer*, **116**(3) pp. 570-576.
- Huber, A. M., and R. Viskanta, 1994b, "Effect of Jet-Jet Spacing on Convective Heat-Transfer to Confined, Impinging Arrays of Axisymmetric Air Jets," *International Journal of Heat and Mass Transfer*, **37**(18) pp. 2857-2869.
- Jambunathan, K., E. Lai, M. A. Moss, and B. L. Button, 1992, "A Review of Heat Transfer Data for Single Circular Jet Impingement," *International Journal of Heat and Fluid Flow*, **13**(2) pp. 106-115.
- Kercher, D. M., and W. Tabakoff, 1970, "Heat Transfer by a Square Array of Round Air Jets Impinging Perpendicular to a Flat Surface Including the Effect of Spent Air," *Journal of Engineering for Power*, **92**(1) pp. 73-82.
- Kline, S. J., and F. A. McClintock, 1953, "Describing Uncertainty in Single-Sample Experiments," *Mechanical Engineering*, **75**(1) pp. 3-8.
- Martin, H., 1977, "Heat and Mass Transfer between Impinging Gas Jets and Solid Surfaces," *Advances in Heat Transfer*, **13** pp. 1-60.
- Onstad, A. J., C. J. Elkins, R. J. Moffat, and J. K. Eaton, 2009, "Flow Measurements and Heat Transfer for a Jet Impingement Array with Local Extraction of the Spent Fluid," *Journal of Heat Transfer*, **131**(7), **To Appear**.
- Rhee, D. H., P. H. Yoon, and H. H. Cho, 2003a, "Local Heat/Mass Transfer and Flow Characteristics of Array Impinging Jets with Effusion Holes Ejecting Spent Air," *International Journal of Heat and Mass Transfer*, **46**(6) pp. 1049-1061.
- Rhee, D. H., J. H. Choi, and H. H. Cho, 2003b, "Heat (Mass) Transfer on Effusion Plate in Impingement/Effusion Cooling Systems," *Journal of Thermophysics and Heat Transfer*, **17**(1) pp. 95-102.
- Viskanta, R., 1993, "Heat Transfer to Impinging Isothermal Gas and Flame Jets," *Experimental Thermal and Fluid Science*, **6**(2) pp. 111-134.